Met. Mater. Int., Vol. 23, No. 1 (2017), pp. 126~131
doi: 10.1007/s12540-017-6109-y

Characterization of γ and γ′ Phases in 2nd and 4th Generation Single Crystal Nickel-Base Superalloys

Maciej Zietara[1,*], Steffen Neumeier[2], Mathias Göken[2], and Aleksandra Czyrska-Filemonowicz[1]

[1]International Centre of Electron Microscopy for Materials Science and Faculty of Metals Engineering and Computer Industrial Science, AGH University of Science and Technology (AGH-UST), PL-30 059 Kraków, Poland
[2]Department Materials Science and Engineering, Friedrich-Alexander-Universität Erlangen-Nürnberg, Institute I, 91058 Erlangen, Germany

(received date: 12 February 2016 / accepted date: 5 July 2016)

A Ni based single crystal superalloy from the 2nd generation, PWA 1484, and one from the 4th generation, PWA 1497, were comparatively studied by scanning electron microscopy, energy dispersive X-ray spectroscopy and nanoindentation technique in an atomic force microscope (NI-AFM) after high temperature creep deformation. During primary creep of both generations of superalloys, γ′ precipitates start to coalesce and grow directionally. Further creep deformation leads to the topological inversion and coarsening of the rafted microstructure. The NI-AFM technique was used for measurements of the hardness of the γ and γ′ phases in as-received and creep deformed samples in various conditions. The g matrix of the PWA 1497 superalloy is on average 0.8 GPa harder than that of PWA 1484 that can be explained by higher content of Re and Ru, since they partition predominantly to the matrix phase.

Keywords: superalloy, NI-AFM, nanoindentation, rafting, creep

1. INTRODUCTION

Single crystal (SC) nickel-base superalloys are mainly applied as turbine blades and vanes in aero-engines and industrial gas turbines. This group of alloys has been constantly developed for over 40 years to increase their superior mechanical properties such as creep resistance and high temperature strength. The microstructure of SC superalloys consists of a high volume fraction of hardening γ′ phase which is coherently precipitated in the γ matrix [1-5].

In the recent years, the coupled nanoindentation atomic force microscope (NI-AFM) technique has become a valuable tool for materials science. The application of this technique is especially promising for precipitation hardening materials with a precipitate size below 1 μm, e.g. for Ni-base superalloys. This technique has been described in Refs [6-9]. In the present research the NI-AFM technique was used for quantitative measurements of the hardness of the γ and γ′ phases. Investigations were performed on selected samples of the PWA1484 and the PWA 1497 superalloys for the as-received samples (after heat treatment) and after creep tests at 982 °C/248 MPa and various strain conditions.

*Corresponding author: zietara@agh.edu.pl

The present study focuses on the detailed characterization of γ and γ′ phases (morphology, chemical composition/partitioning, nanohardness) of 2nd and 4th generation SC superalloys and their microstructural changes during creep deformation at high temperature. We correlate the microscopic and spectroscopic findings with the hardness of the phases with the intention of a better understanding of the microstructural parameters that influence the creep behavior of SC superalloys.

2. EXPERIMENTAL PROCEDURE

2.1. Investigated materials

Two nickel-base SC superalloys were investigated: PWA 1484, a typical second generation single crystal superalloy and PWA 1497, a fourth generation single crystal superalloy. The chemical compositions of both superalloys are presented in Table 1. Both PWA 1484 and PWA 1497 superalloys were solidified into single crystals. Bars with orientations within 5° of the <001> casting direction were selected for mechanical testing to minimize the effect of orientation on the results. The solid bars of the PWA 1484 and PWA 1497 superalloys were subjected to the customary heat treatment, involving solution annealing followed by ageing. Further experimental details are given in Ref. [5].

Table 1. Chemical compositions of the PWA 1484 and the PWA 1497 alloys (Ni-bal., wt%)

Alloy	Cr	Co	Mo	Re	Ru	W	Al	Ta	Hf	B
PWA 1484	5.0	10.0	2.0	3.0	-	6.0	5.6	8.7	0.1	-
PWA 1497	2.0	16.5	2.0	5.95	3.0	6.0	5.55	8.25	0.15	40 ppm

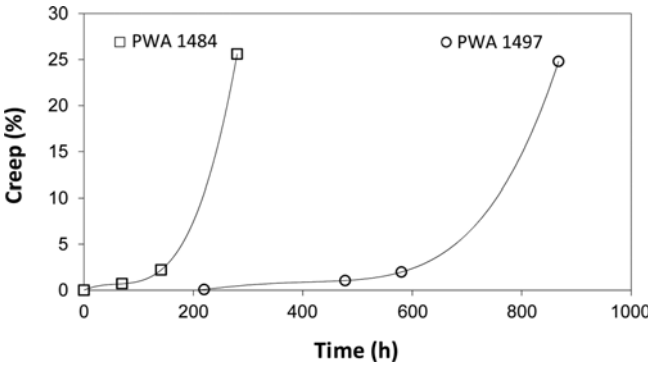

Fig. 1. Creep curves of PWA 1484 and PWA 1497 superalloys, deformed at 982 °C and constant load of 248 MPa [5]. Hardness measurements were conducted on creep-interrupted specimens, as marked at both creep curves.

2.2. Creep tests

Six specimens (three of PWA 1484 and three of PWA 1497) were creep tested at the same temperature 982 °C and constant load of 248 MPa. In order to avoid recovery processes the specimens were cooled under load. One sample from each alloy was creep tested until rupture. All creep tests were performed by the Institute of Aviation in Warsaw. The creep strain curves of the PWA 1484 and the PWA 1497 superalloys deformed under the same conditions are presented in Fig. 1 [5].

2.3. Sample preparation

All samples were prepared and treated in the same manner to minimize the influence of sample preparation on the results. All samples were cut into small pieces with special care to obtain the same crystallographic orientations, (010) or (100). To set the same orientation of the samples, cutting was performed along the axis of primary dendrite arms. Sample preparation for Scanning Electron Microscope (SEM) analyses included low-speed diamond saw cutting, mechanical polishing with diamond and silica suspended solids. To reveal details of the microstructure, chemical etching in a solution of a γ′- dissolving agent: 25 ml ethanol + 25 ml HNO_3 + 27 ml HCl at room temperature was performed. Transmission Electron Microscopy (TEM) sample preparation include electrochemical polishing using double-jet Struers TenuPol 3, solution: 450 ml $CH_2OHCH_2OC_4H_9$ + 450 ml CH_3COOH + 100 ml $HCLO_4$, process parameters were: temperature -4 °C, voltage 26 V. Sample preparation for NI-AFM technique included low-speed diamond saw cutting, and two-stage polishing; first standard mechanical polishing by using diamond suspended solids and final chemo-mechanical polishing with 0.125 μm silica suspended solids. Final chemo-mechanical polishing allows a smooth surface to be produced, with a small height difference between γ and γ′ phases in superalloys, which produces contrast in AFM.

2.4. SEM and TEM examination

SEM microstructural examination was carried out using a Merlin Gemini II (ZEISS) microscope. TEM examination and Energy dispersive X-ray spectroscopy (EDX) analysis was carried out using TITAN G2 60-300 (FEI) equipped with ChemiStem system.

2.5. NI-AFM examination

The NI-AFM examination were carried out at room temperature using a Veeco Instruments Multimode atomic force microscope equipped with an add-on Triboscope force transducer from Hysitron. The transducer, mounted on a conventional AFM, controls the *z*-movement of the tip and measures the indentation force. In all indentation experiments a diamond cube corner tip (three sided pyramid) with a tip angle of 90° was used. The same diamond tip was used to image the topography of the sample surfaces. All indentations in the γ matrix phase (in the initial microstructures of both superalloys γ matrix channels are very narrow) were performed in the cross-section of matrix channels lying perpendicular to the surface of the samples.

The hardness (H) was derived from the nanoindentation experiments by evaluation of the load-displacement curve according to the Oliver-Pharr method [10]. The hardness H is calculated from $H = P_{max}/A_c$ equation, where P_{max} is the maximum force during indentation and A_c the projected contact area. The maximum force during indentation was kept constant at 250 μN. To secure proper statistics, ten measurements were performed for each phase (γ or γ′) in each sample.

3. RESULTS AND DISCUSSION

Figures 2 and 3 show the microstructures and EDX elemental maps of PWA 1484 and PWA1497, respectively. SEM analysis of the as-received PWA1484 and PWA1497 superalloy samples revealed a regular cuboidal morphology of γ′ particles separated by γ channels. TEM-EDX elemental mapping revealed the chemical element partitioning in both phases of PWA 1484 and PWA 1497 superalloys. Elemental maps for the 2nd generation superalloy is shown in Fig. 2(b) and for the 4th generation superalloy in Fig. 3(b) respectively. It was established

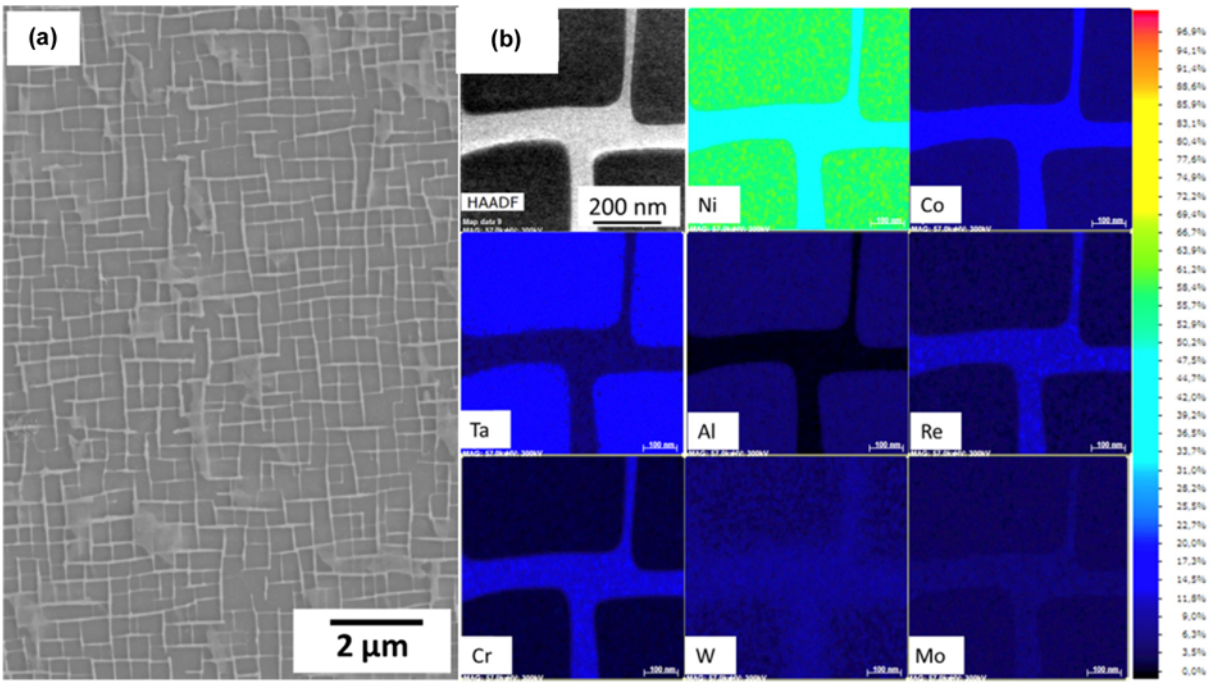

Fig. 2. Microstructure of as-received PWA 1484 (a), SEM image detail (b); STEM-HAADF EDX elemental maps.

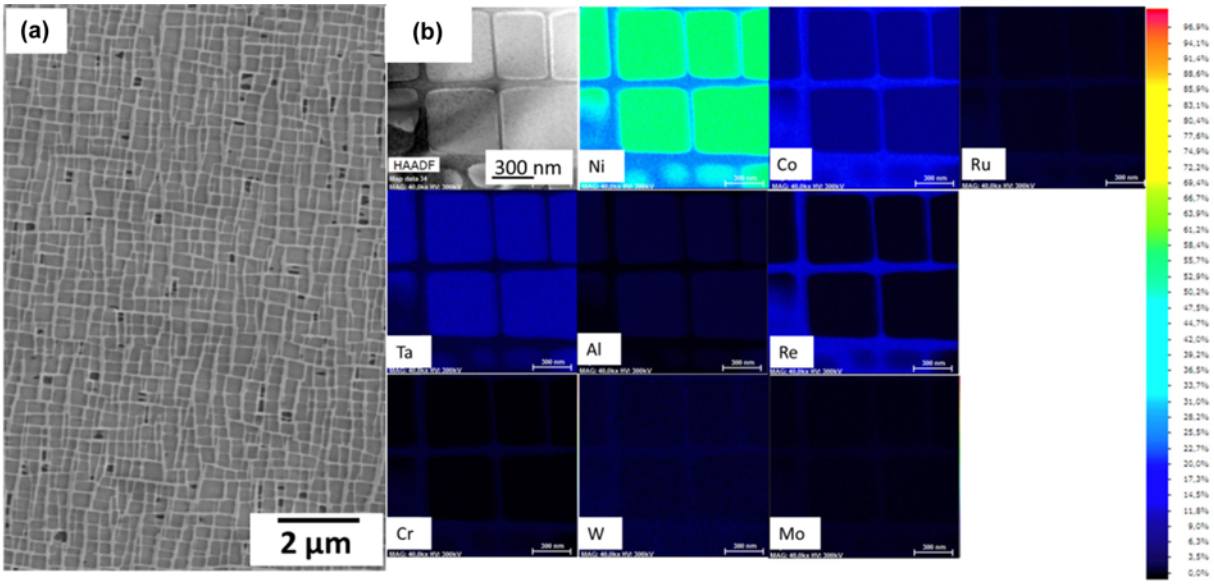

Fig. 3. Microstructure of as-received PWA 1497 (a), SEM image detail (b); STEM-HAADF EDX elemental maps.

that the matrix of 2nd generation PWA 1484 contains mainly Ni, Cr, Mo, W, Co and Re, while 4th generation PWA 1497 contains also Ru. The same effect of Ru partitions to the γ matrix was found by Peng *et al.* [11], who investigated by Atomic Probe Tomography an experimental superalloy Astral 21 containing 1 at% Ru derived from CMSX-4 (2nd generation). The γ′ particles precipitated in both superalloys contain mainly Ni, Al and Ta. During high temperature creep deformation, the initially cubic-shaped precipitates transform under the influence of stress and temperature into plates (rafts). The rafts develop in the early stages of creep (Figs 4 and 5). Simultaneously with the rafting process, a thickening of the γ matrix channels parallel to the rafts occurs.

Figure 6 shows PWA 1484 (a) and PWA 1497 (b) superalloys surface topography revealed by AFM after hardness measurements. Figure 6 further shows the evolution of the microstructure which is called "topological inversion". The γ′ phase coalesces, coarsens and finally surrounds the γ phase, thereby becoming topologically the matrix [3,12].

Ten indents for each phase (γ and γ′) were performed for

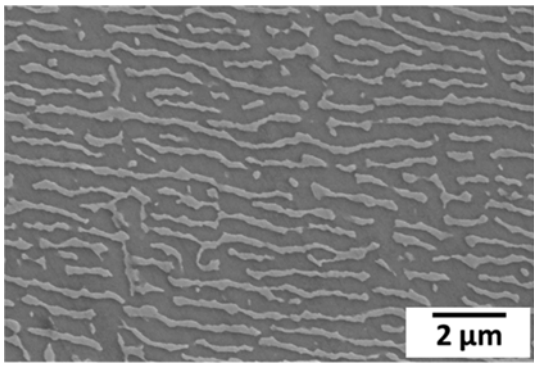

Fig. 4. SEM image of PWA 1484 creep deformed at 982 °C/248MPa to a creep strain of 1.5% for 140 h.

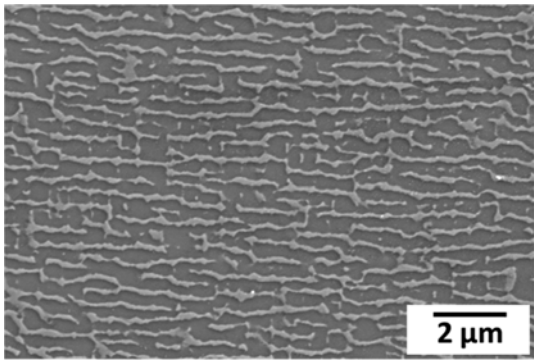

Fig. 5. SEM image of PWA 1497 creep deformed at 982 °C/248MPa to a creep strain of 0.85% for 480 h.

each sample. The scan size for each AFM micrograph is 10 µm × 10 µm. Brighter colour indicates γ matrix phase and γ′ phase precipitates are represented by darker shade, the contrast is obtained due to differences in height on the surface of

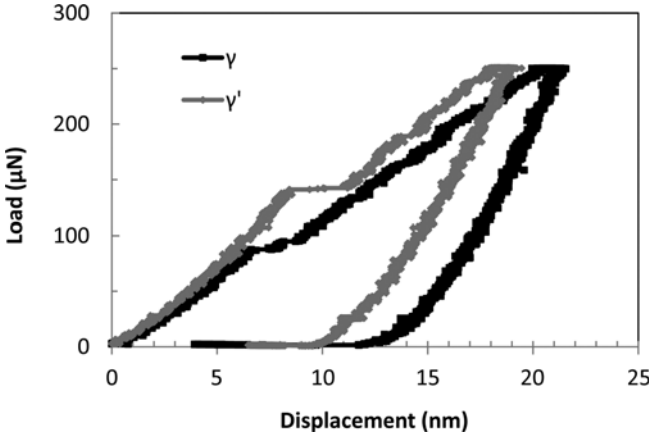

Fig. 7. The exemplary load-displacement curves of the γ matrix and γ′ phase for PWA 1497 superalloy.

the samples which are caused by difference in chemo-mechanical behavior of the phases. Exemplary load-displacement curves of the γ matrix and γ′ phase of PWA 1497 superalloy are shown in Fig. 7.

To understand the change in hardness of the of the γ and γ′ phases in PWA1484 and PWA1497 superalloys the partitioning behavior of the alloying elements was calculated. The partitioning behavior of the alloying elements via the partitioning coefficient k is shown in Fig. 8.

The comparison of the mean hardness of both phases in each superalloy in the as-received state (see Fig. 9) shows that the precipitates of the γ′ phase are always harder than the γ matrix phase. This is mainly due to the chemical composition and the structure of both phases. The hardness of the γ′ precipitates of the as-received PWA 1484 superalloy is slightly higher than the hardness of the γ′ phase of PWA 1497. It might

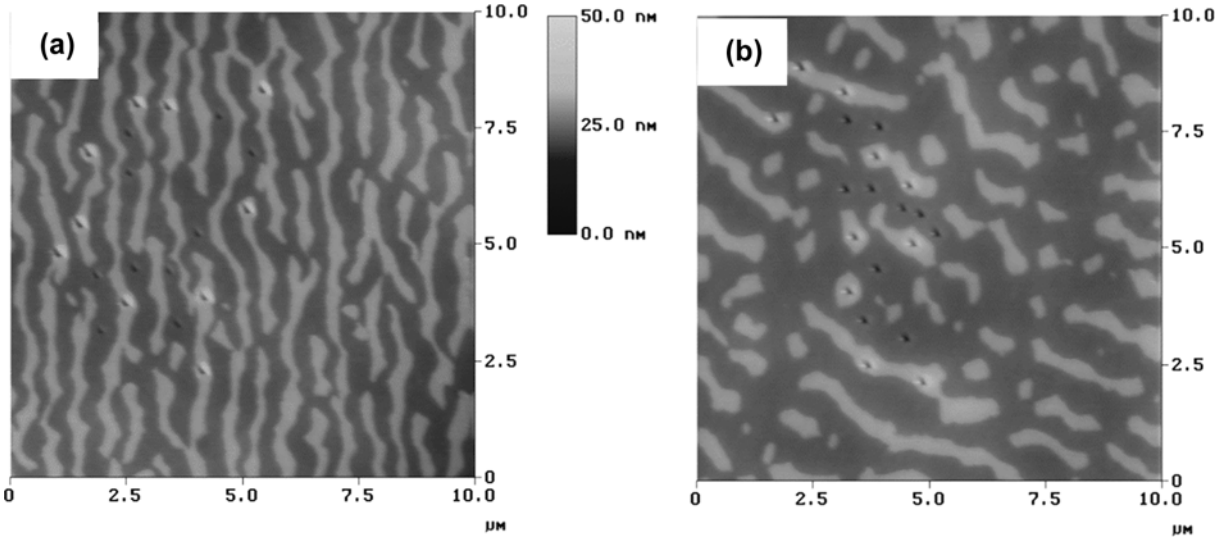

Fig. 6. Samples of PWA 1484 (a) and PWA 1497 (b) superalloys, creep tested until rupture at 982 °C/248 MPa: surface topography after NI-AFM tests (indents in γ and γ′ phases are visible) revealed by AFM.

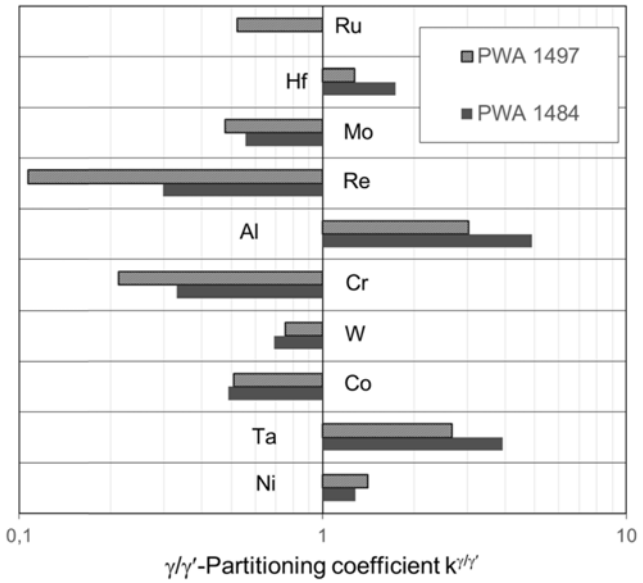

Fig. 8. Partitioning coefficient $k^{\gamma'/\gamma}$ of the alloying elements in the PWA1484 and PWA 1497 superalloys.

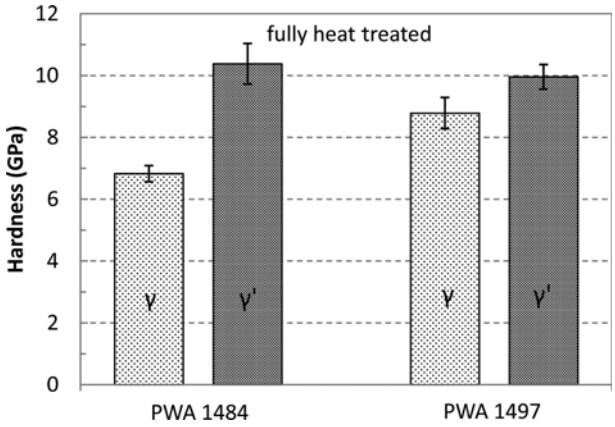

Fig. 9. Hardness of γ and γ′ phase of PWA 1484 and PWA1497 in the as-received condition.

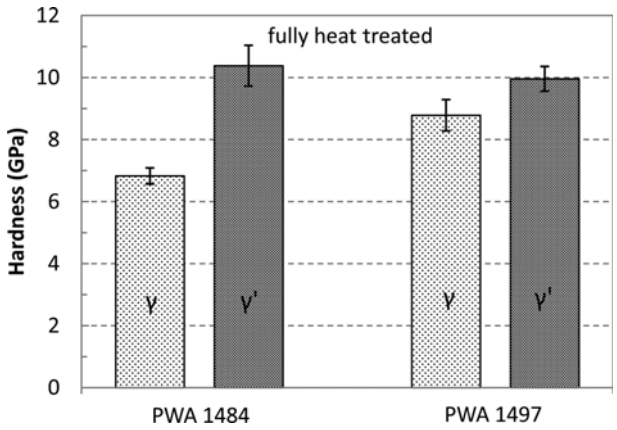

Fig. 10. Comparison of the mean γ and γ′ hardness of PWA 1484 and PWA 1497 after creep deformation.

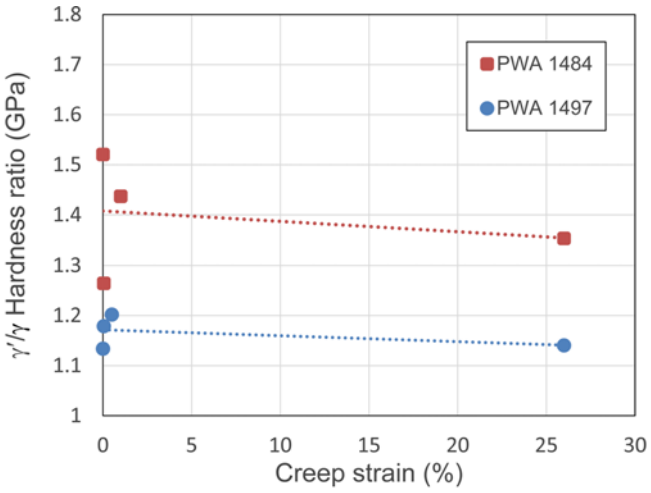

Fig. 11. Hardness ratio as a function of creep strain for of PWA 1484 and PWA 1497.

be due to the difference in chemical composition of both alloys; PWA 1497 contains less Ta which act as a strengthening element for the γ′ phase.

In contrary to the γ′ phase the γ matrix of the PWA 1497 superalloy is significantly harder than that of PWA 1484 that might be explained by higher content of Re and addition of Ru, since they partition predominantly to the matrix phase, as shown by EDX analysis of the matrix in both superalloys (Figs 2b and 3b). Similar results were presented by Durst and Göken [7] who compared the hardness of γ and γ′ in 1st (CMSX-6), 2nd (CMSX-4) and 3rd (CMSX-10) generation of the SC superalloys. According to Durst *et al.* [7]. the different generations of SC nickel-base superalloys clearly show an increased hardness of the γ matrix with a higher concentration of rhenium, while no significant difference in the hardness of the γ′ precipitates could be found. Hence, the higher stability of 4th generation superalloy PWA 1497 is related to significantly stronger solid solution strengthening (among others, by Re and Ru), which results in higher hardness of γ matrix in comparison with that of 2nd generation PWA 1484 superalloy. This leads also to increased creep strength at high temperatures because creep deformation is controlled mostly by dislocation climb in the γ phase. During high temperature creep deformation interfacial dislocations are formed, coherency stresses are relieved, microstructural coarsening and rafting of γ and γ′ occurs (see Figs. 4 and 5), however the γ matrix of PWA 1497 still contains a higher concentration of solid solution strengthening elements Re and Ru. This explains why the γ matrix of crept PWA 1497 is still harder compared to the γ matrix of crept PWA 1484 (see Fig. 10). Durst *et al.* [7] as well as Neumeier *et al.* [12] concluded that the gamma hardness increases only by about 0.5-0.6GPa if the content of Re is increased by 3 wt%, i.e. if we go from the second

generation Ni-base superalloys CMSX-4 to the third generation alloy CMSX-10. However, if we compare the initial states as well as the crept states of PWA 1484 and PWA 1497, we see a larger increase in hardness by adding 3 wt% Re and 3 wt% Ru, which seems to be an effect of the additional content of Ru. Since Ru partitions predominantly to gamma and is known to have a strengthening effect on Ni, (see Fig. 8), [13], it is reasonable to assume that Ru contributes also to the increased hardness of PWA 1497 superalloy.

Since there is no tendency or clear difference in the hardness of and γ′ phase in the samples after different creep deformation of both superalloys only the average hardness values of γ and γ′ after the different creep strains are shown in Fig. 10. The hardness ratio as a function of creep strain for both alloys is shown in Fig. 11.

4. SUMMARY

The microstructure of 2nd and 4th generation SC superalloys (as-received and creep-deformed samples) was characterized by SEM, STEM-HAADF-EDX and NI-AFM techniques. The nanoindentation hardness measurements reveal similar results for as-received as well as crept samples. The hardness of the γ′ phase of the PWA 1484 superalloy is slightly higher than the hardness of the γ′ phase of the PWA 1497, while the γ matrix of the PWA 1497 superalloy is significantly harder than that of PWA 1484. This is due to the higher content of rhenium and ruthenium, since they partition predominantly to the γ phase and act as solid solution strengthening elements.

ACKNOWLEDGMENTS

This work was supported by the Polish Ministry of Science and Higher Education (project nr 11.11.110.299), within the AGH-UST statutory research.

REFERENCES

1. R. C. Reed, *The Superalloys: Fundamentals and Application*, p. 1, Cambridge University Press, Cambridge, UK (2006).
2. A. Czyrska-Filemonowicz, B. Dubiel, M. Zietara, and A. Cetel, *Inżynieria Materiałowa* **3-4**, 128 (2007).
3. M. Zietara, A. Cetel, and A. Czyrska-Filemonowicz, *Mater. Trans.* **52**, 336 (2011).
4. M. Zietara, A. Kruk, A. Gruszczyński, and A. Czyrska-Filemonowicz, *Mater. Charact.* **87**, 143 (2014).
5. M. Zietara, *Ph. D. Thesis*, pp.1, 30-90, AGH University of Science and Technology, Poland (2011).
6. M. Göken and M. Kempf, *Acta Mater.* **47**, 1043 (1999).
7. K. Durst and M. Göken, *Mat. Sci. Eng. A* **387-389**, 312 (2004).
8. S. Neumeier, M. Dinkel, F. Pyczak, and M. Göken, *Mat. Sci. Eng. A* **528**, 815 (2011).
9. H. Rehman, K. Durst, S. Neumeier, and A. Parsa, *Mat. Sci. Eng. A* **634**,202 (2015).
10. W. C. Oliver and G. M. Pharr, *J. Mater. Res.* **7**, 1564 (1992).
11. Z. Peng, I. Povstugar, K. Matuszewski, R. Rettig, R. Singer, P. Choi, *et al. Scripta Mater.* **101**, 44 (2015).
12. S. Neumeier, F. Pyczak, and M. Göken, *Philos. Mag.* **91**, 4187 (2011).
13. A. Epishin, T. Link, U. Brückner, and P.D. Portella, *Acta Mater.* **49**, 4017 (2001).
14. H. A. Roth, C. L. Davis, and R. C. Thomson, *Metall. Mater. Trans. A* **28**, 1329 (1997).